

Electronic Supplementary Information

Diffusion of Bulky Organic Cations in the 3D/2D Heterostructures to Form Interfacial Quasi-2D (N2) Phase for Tin Perovskite Solar Cells

Ashank Seetharaman,^a Sudhakar Narra,^{ab} Parameswaran Rajamanickam,^c
Raghunath Putikam,^a Ming-Chang Lin^a and Eric Wei-Guang Diau^{*ab}

a. Department of Applied Chemistry and Institute of Molecular Science, National Yang Ming Chiao Tung University, 1001 Ta-Hseuh Rd., Hsinchu 30010, Taiwan.

*Correspondence author. Email: diaw@nycu.edu.tw

b. Center for Emergent Functional Matter Science, National Yang Ming Chiao Tung University, 1001 Ta-Hseuh Rd., Hsinchu 30010, Taiwan.

c. Department of Materials Science and Engineering, National Yang Ming Chiao Tung University, 1001 Ta-Hseuh Rd., Hsinchu 30010, Taiwan.

Materials

Tin iodide (SnI_2 , 99%, Alfa Aesar), tin fluoride (SnF_2 , 99%, Sigma Aldrich), formamidinium iodide (FAI, Greatcell Solar), ethylene diammonium diiodide (EDAI_2 , Greatcell Solar), n-butyl ammonium iodide (BAI, Greatcell Solar), phenethylammonium iodide (PEA, Greatcell Solar), n-Hexylammonium iodide (HAI, Greatcell Solar), n-Octylammonium Iodide (OAI, Greatcell Solar) tin powder (Alfa Aesar), dimethyl sulfoxide (DMSO, Sigma Aldrich), dimethyl formamide (DMF, Sigma Aldrich), isopropyl alcohol (IPA, Sigma Aldrich) and chlorobenzene (CB, Sigma Aldrich) were used as received.

Perovskite film preparation for photophysical characterizations

The perovskite inks and films were prepared inside a N_2 -filled glove box ($\text{O}_2 \leq 2$ ppm, $\text{H}_2\text{O} \leq 0.5$ ppm). The E1 ($\text{FASnI}_3 + 1\% \text{EDAI}_2$) perovskite ink was prepared by dissolving 372.5 mg of SnI_2 , 15.7 mg of SnF_2 , 3.2 mg of EDAI_2 , 168.5 mg of FAI, and about 40 – 50 mg of tin powder in 1.22 mL of DMSO. The N1 perovskite ink was prepared by mixing 93.1 mg of SnI_2 , 4 mg of SnF_2 , and 100.5 mg of BAI / 124.5 mg of PEAI in 313 μL of DMSO, / 114.5 mg of HAI in 313 μL of DMF, / 128.58 mg of OAI in 2.5 ml of IPA along with 15 – 20 mg of tin powder while the N2 ink was prepared by dissolving 93.1 mg of SnI_2 , 4 mg of SnF_2 , 21.5 mg of FAI, 50.3 mg of BAI, and 15 – 20 mg of tin powder in 313 μL of DMSO. The perovskite films (E1, N1, and N2) were developed onto cleaned circular glass substrates of diameter ~ 25.4 mm and thickness ~ 1 mm, that were treated with UV ozone for 30 min. For E1 perovskite deposition, about 18 μL of the prepared E1 solution was loaded and evenly spread over the substrate, followed by spin-coating (5000 rpm for 90 s). Chlorobenzene (750 μL), as an antisolvent, was quickly injected after 60 s past-initiation of the spinning process. Thereafter, the obtained reddish film was annealed at 70 $^\circ\text{C}$ for 10 min on a hot plate.^{1, 2} For N1(BA/HA/PEA) deposition, the glass substrates were spin-coated with 18 μL of the prepared N1 ink (8000 rpm for 56 s), with chlorobenzene (650 μL) injected as an antisolvent after 34 s from the start of the spinning process whereas no antisolvent was introduced for N1(OA). The spin-coated films were annealed at 70 $^\circ\text{C}$ for 10 min on a hot plate. Finally, N2 thin films were prepared by spin-coating 16 μL of the prepared N2 ink (5000 rpm, 53 s), where chlorobenzene (650 μL) was injected after 31 s from the commencement of the spinning process.

Finally, the N2 films were also annealed at 70 °C for 10 min. The films were then encapsulated using cleaned circular glass substrate by applying optical adhesive (Norland 61, Thorlabs NOA61), followed by curing with UV light.

Perovskite heterostructure formation

The pristine E1 and N1 films formed on independent glass substrates were stacked on top of each other, held with a forceps, and encapsulated by applying optical adhesive (Norland 61, Thorlabs NOA61), at the joining edges and cured with UV light. The forceps was removed after 10 minutes when the encapsulation was completed. The applied pressure was estimated using Force sensing resistor (FSR 402, interlink electronics) with a sensing diameter of 1.27 cm and Arduino UNO micro controller. The pressure applied is estimated to be 160 kPa.

Perovskite film preparation for, UPS and SEM

The pristine E1, N1 and N2 films were prepared on ITO glass substrates for improving the conductivity.

Solar cell fabrication

Commercial ITO glass substrates (1.9x1.9 cm²) were thoroughly washed and oven-dried before using. The dried substrates were subjected to oxygen plasma for 20 min, followed by deposition of PEDOT:PSS through spin-coating technique (5000 rpm, 60 s), and then annealed at 150°C for 10 min. Subsequently, the films were transferred to a nitrogen filled glovebox (O₂ ≤ 2 ppm, H₂O ≤ 0.5 ppm) for depositing perovskite layers. The E1 and N1(BA) perovskite deposition were performed as described previously, except, for the device fabrication, the PEDOT:PSS-coated ITO substrates were employed instead of circular glass substrates. The formed E1 and N1(BA) films were used to establish heterostructure as soon as the annealing is over using forceps as described in the text. Then, they were carefully packed and sealed inside the glovebox for 4 days and 15 days, after which they were split to get E1N1/E1 and E1N1/N1 films. The E1N1/E1 films were eventually transferred to the thermal evaporation chamber for subsequent layer deposition (C₆₀ ~35 nm, BCP ~5 nm, and silver ~100 nm) at ultra-high vacuum condition. For

reference, freshly prepared pristine E1 films were also used to deposit C₆₀ as an electron-transport layer, BCP as a hole-blocking layer, and silver as a back-contact electrode.

Structural characterizations

Ultraviolet photoelectron spectra (UPS), for pristine samples, were measured using Thermo Fisher Scientific, ESCALAB Xi+. The samples were biased at -5.0 V to avoid the overlap of low-energy secondary electron cut-off signals of the instrument. The Fermi edge of a clean gold surface was used for calibration. The measurement was done under 10⁻⁹ Torr pressure. The calculated valence band positions are close to the reported values.^{1, 3, 4} Field emission scanning electron microscope (FESEM, Hitachi SU8010) was used to image the morphology of the samples and the images were post-processed for better contrast/brightness. X-ray diffraction (XRD) was recorded using D8 Discover X-ray Diffraction System, Bruker.

Photophysical characterizations

The absorbance measurements were done using JASCO spectrophotometer (V-780) equipped with an integration sphere (ISN-9011, JASCO). For the photoluminescence (PL) measurements, the samples were excited with CW diode laser (450 nm, MDL-III-450-100 mW; power supply: PSU-III-FDA) which is modulated at a frequency of 300 Hz and the emission was collected using a monochromator (Dongwoo, DM150i, blaze at 750 nm; groove density 600 gr/mm) and Si-photodiode detector (TE cooled, Sciencetech Inc. S-025-TE2-H; power supply PS/TC-1). The signal from the detector was coupled to a digital multimeter (DMM4020) followed by a lock-in amplifier (Zurich Instruments, MFLI 500 kHz/5 MHz, 60 MSa/s, 16 bits). The PL spectra were measured by scanning the grating of the monochromator on a wavelength scale in increments of 6 nm.

For external effect (light and heat), the N1 side of the stacked sample was subjected to one Sun optical power, which was calibrated using a standard Si photodiode (S1337-1012 BQ, Hamamatsu), and the E1 side was placed on a hotplate. The hotplate temperature was set to 50 °C.

Femtosecond Transient absorption spectrometer (fs-TAS)

The fs-TAS measurements were done with an optical setup consisting of ultra-rapid amplified laser system and pump-probe spectrometer (ExciPro, CDP).⁵ The ultrashort laser pulses generated with a Ti-sapphire amplifier system (Coherent, Legend USP, 1 kHz, 795 nm, 3 mJ, 45 fs) was split into two parts using a beam splitter and was directed to two TOPAS-C to generate pump and probe light. The pump light from one of the TOPAS-C (pulse width of 150 fs) was used to excite perovskite samples with different excitation wavelengths. Similarly, probe light of 1300 nm wavelength was generated from another TOPAS-C which was used to pump a sapphire crystal (thickness 5 mm) to generate white-light continuum pulse. The probe wavelength range was limited to 550 – 989 nm using a bandpass filter (Newport 10 SWF-1050-B). The optical alignment for the pump and probe beam overlap was done to have non-collinear geometry at the sample position. Chirp measurement was done using glass substrates to account for the dispersion in white light continuum generation to correct the time zero for each wavelength.⁶ The laser fluences varies between 10 and 25 $\mu\text{J cm}^{-2}$ to obtain similar ΔA values.

Photovoltaic characterizations

The current density-voltage (J - V) curves were recorded under one-sun illumination (AM 1.5G, 100 mW cm^{-2}) using Keithley 2400 digital source meter, from a solar simulator (XES-40S1, SAN-E1) that was calibrated with a reference silicon cell (Oriel, PN 91150V, VLSI standard) to adjust any mismatch in the spectrum. A metal mask was used during the J - V measurement to expose only an area of 0.0225 cm^2 . The Incident Photon-to-Current Conversion Efficiency (IPCE) spectra were obtained from a system powered by a Xe source lamp (A-1010, PTi, 150 W), and a monochromator (PTi). Prior to the measurement, the system was calibrated using a standard Si photodiode (S1337-1012 BQ, Hamamatsu). The device measurements were performed in ambient conditions. The photovoltaic parameters are tabulated in Table S2.

Computational methods

The electronic structure optimizations of FASnI_3 (3D), $\text{BA}_2 \text{FA}_{(n-1)} \text{Sn}_n \text{I}_{(3n+1)}$ (2D, $n = 1-6$, N1-N6) and 3D-2D heterostructures namely 3D-N1 and 3D-N2-N1, were performed using the Vienna ab

initio simulation package (VASP).⁷ The total energies were estimated using the exchange-correlation functional described by generalized gradient approximation (GGA) parameterized by the Perdew-Burke-Ernzerhof formulation (PBE).⁸ The valence electron configurations considered in this calculation are Sn($4d^{10}5s^25p^2$), I($5s^25p^5$), C($2s^22p^2$), N($2s^22p^3$) and H($1s$). The *van der Waals* interactions between organic components (formamidinium and butyl ammonium cations) and perovskite were accounted by utilizing the standard PBE functional augmented by DFT-D3 method of Grimme with zero-damping function.⁹ The convergence criterion for the self-consistent iteration was set to 1×10^{-4} eV. The cutoff energy for the plane wave basis function was set to 400 eV for all calculations. The *k*-points used for structural optimization and electronic properties calculations were obtained by calculating the Brillouin zone integrals over regular Monkhorst-Pack grids of sizes $5 \times 5 \times 3$ (3D); $3 \times 3 \times 1$ (N1-N6); $2 \times 2 \times 1$ (3D-N1, 3D-N2-N1) for respective structures as indicated in the parenthesis. The atomic positions of atoms and lattice constants of atoms were fully relaxed during structural optimization with a forced convergence of 0.02 eV \AA^{-1} .

Model structures

DFT calculations were performed on pristine 3D, N1 and their heterostructures namely 3D-N1, 3D-N2-N1 samples to study the structural and electronic properties of heterostructure samples and thereby to understand the impacts of templating effects of the 2D structures on the 3D structures. DFT structural optimizations show that pristine 3D sample is tetragonal while all others are orthorhombic. The optimized geometries are shown in Fig. S6 and the lattice parameters are tabulated in Table S1. The lattice parameters of heterostructure samples were shown to be in between that of 3D and N1 samples along a and b directions while the lattice parameters of 3D-N2-N1 samples along c-direction show slight shrinkage in length compared with 3D-N1 due to penetration of the BA chains into 3D dimensional network. The crystal structures and lattice parameters of FASnI_3 and BA_2SnI_4 matches with of the reported results.¹⁰

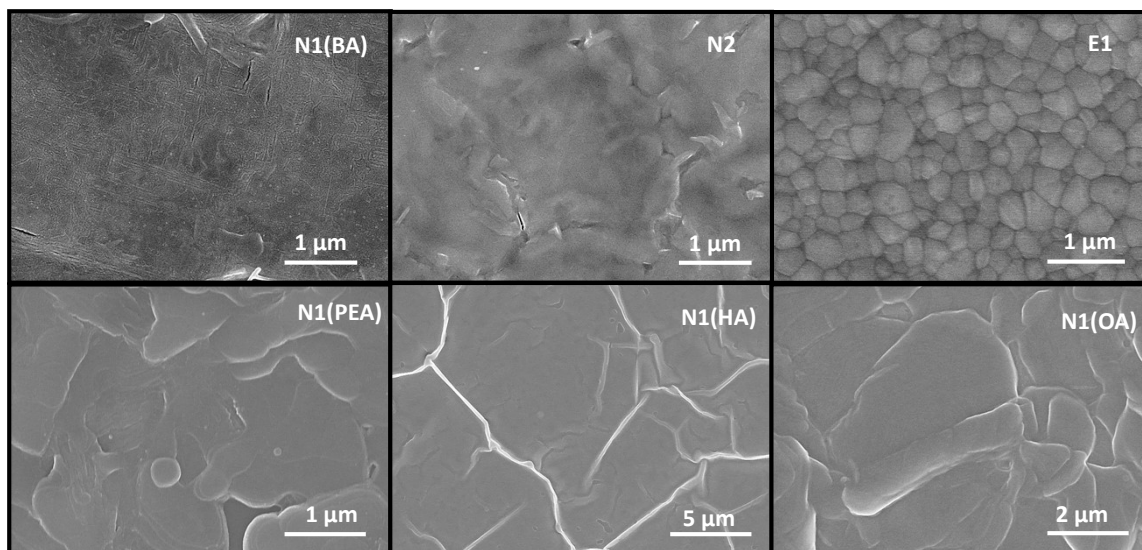


Fig. S1 SEM images for pristine samples - N1(BA), N1(HA), N1(OA), N1(PEA), N2 and E1.

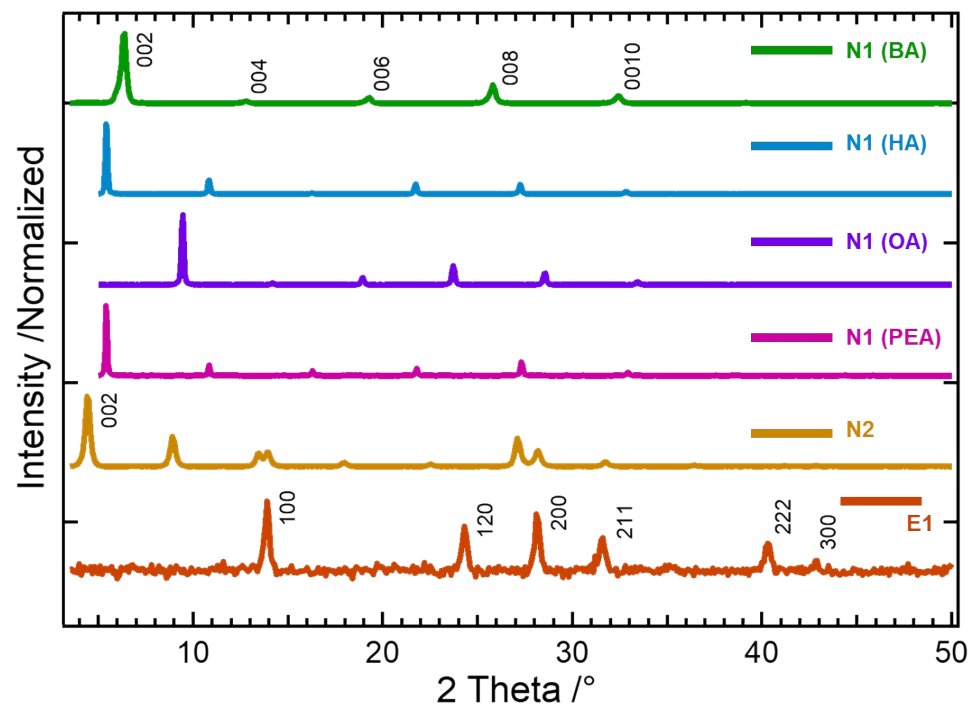


Fig. S2 XRD patterns for pristine samples - N1(BA), N1(HA), NA(OA), N1(PEA), N2 and E1.

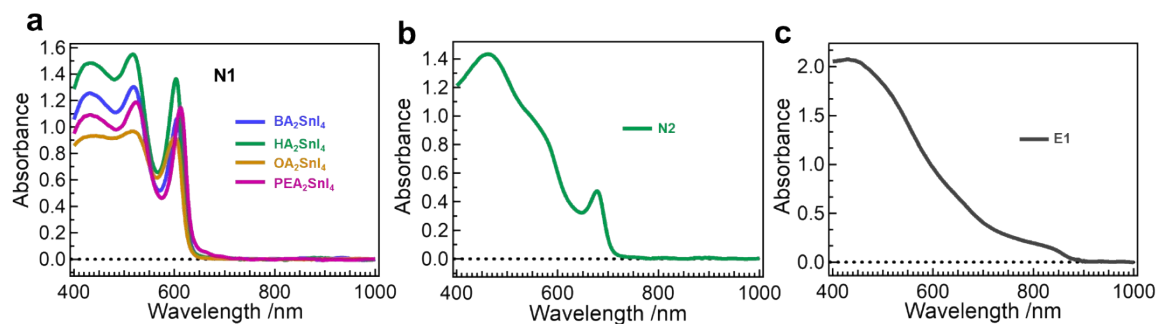


Fig. S3 Steady-state absorption spectra of (a) N1 (BA/HA/OA/PEA), (b) N2, (c) E1.

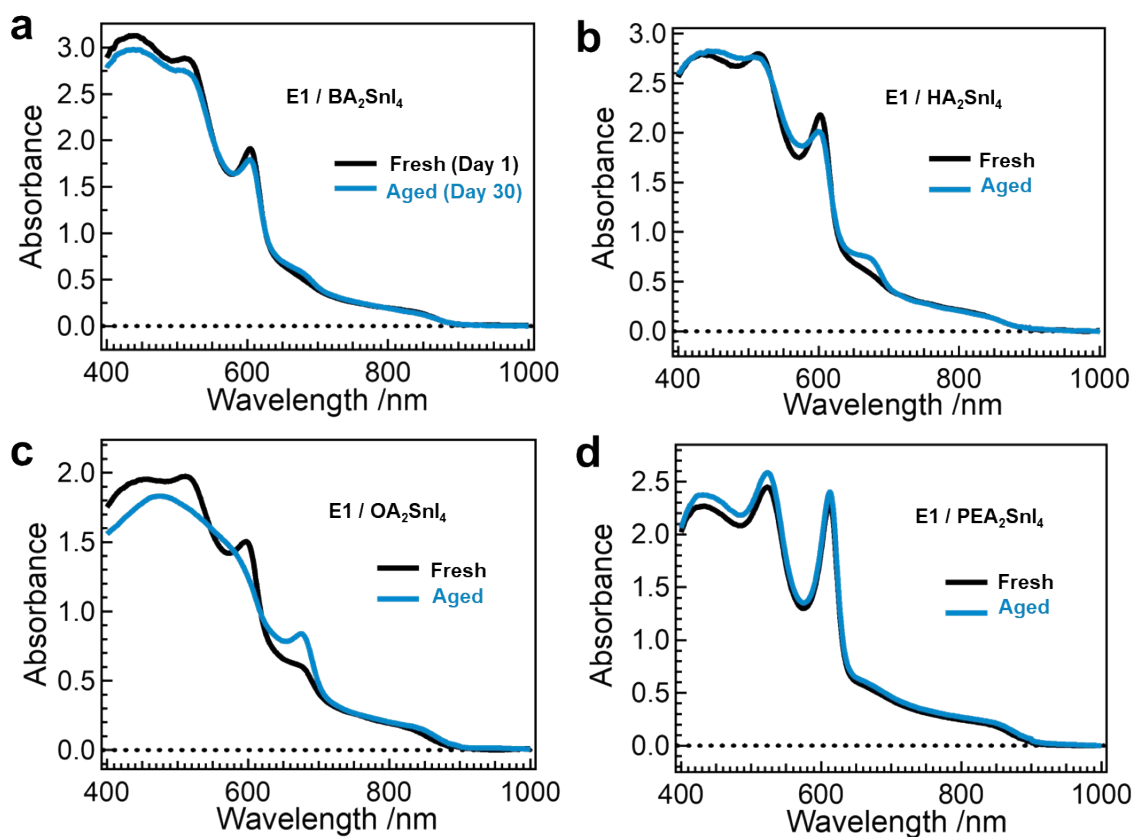


Fig. S4 Steady-state absorption spectra of fresh (Day 1) and aged (Day 30) samples (a) E1N1-BA, (b) E1N1-HA, (c) E1N1-OA, and (d) E1N1-PEA.

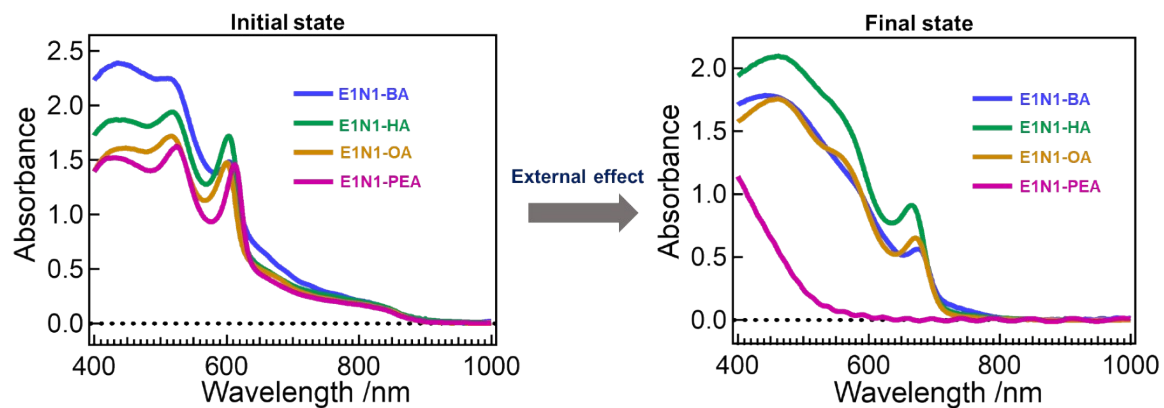
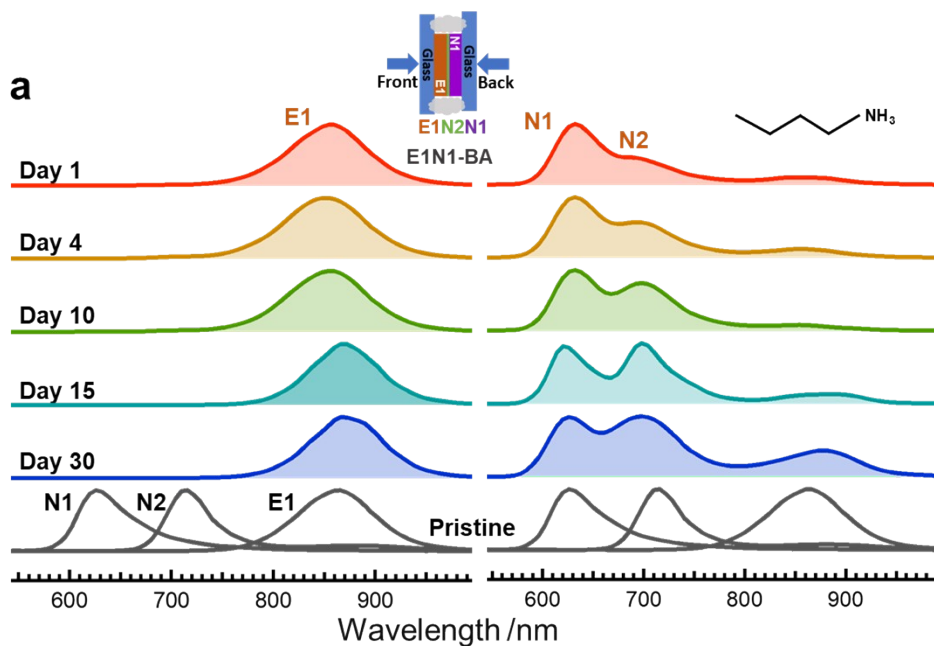
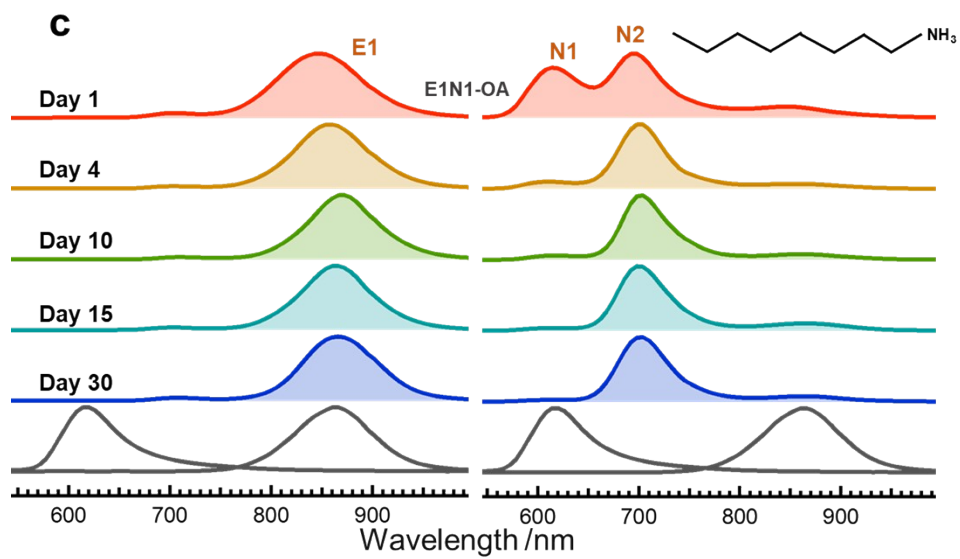
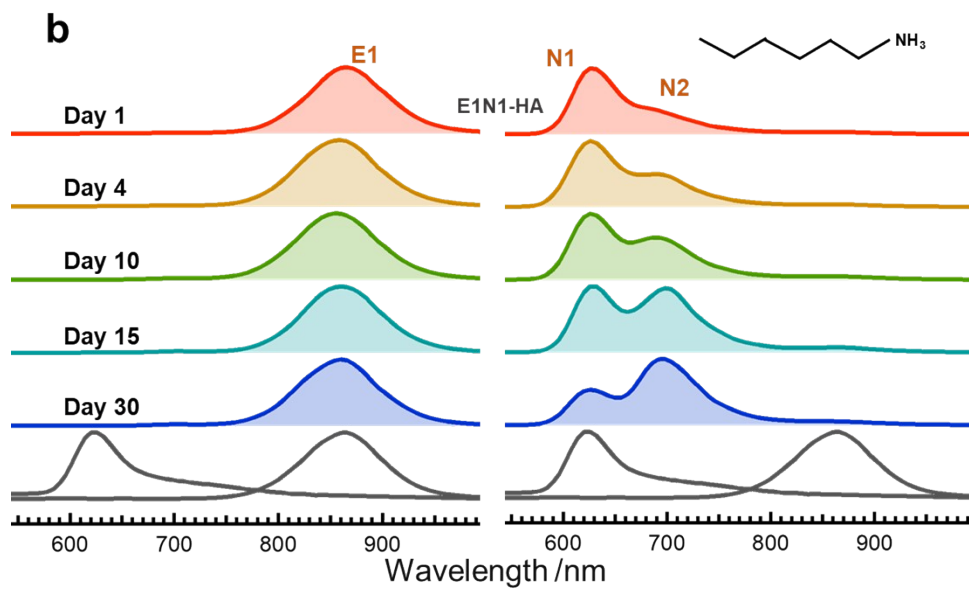


Fig. S5 Steady-state absorption spectra under 1 Sun and 50 °C temperature.





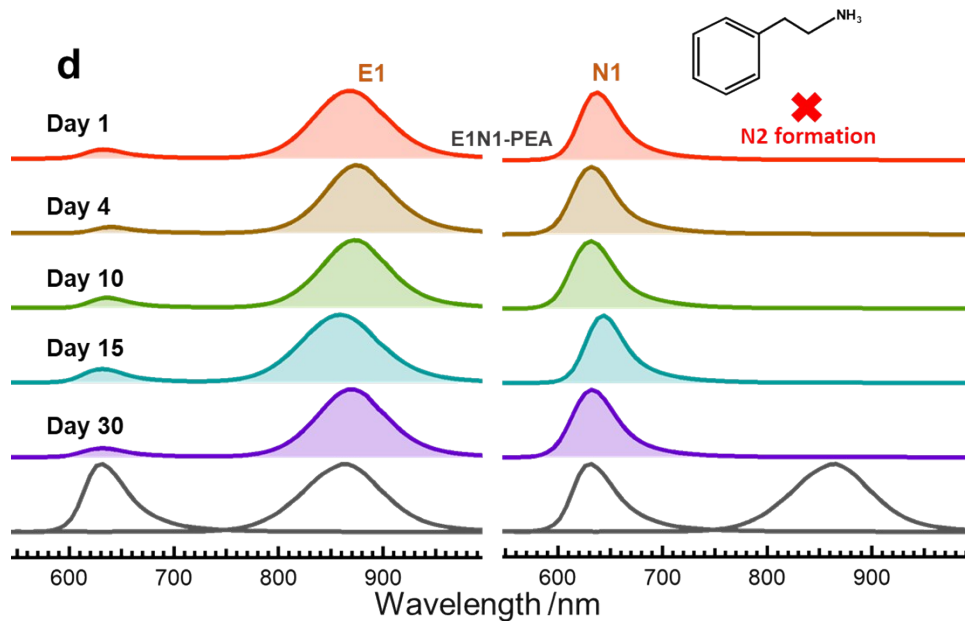
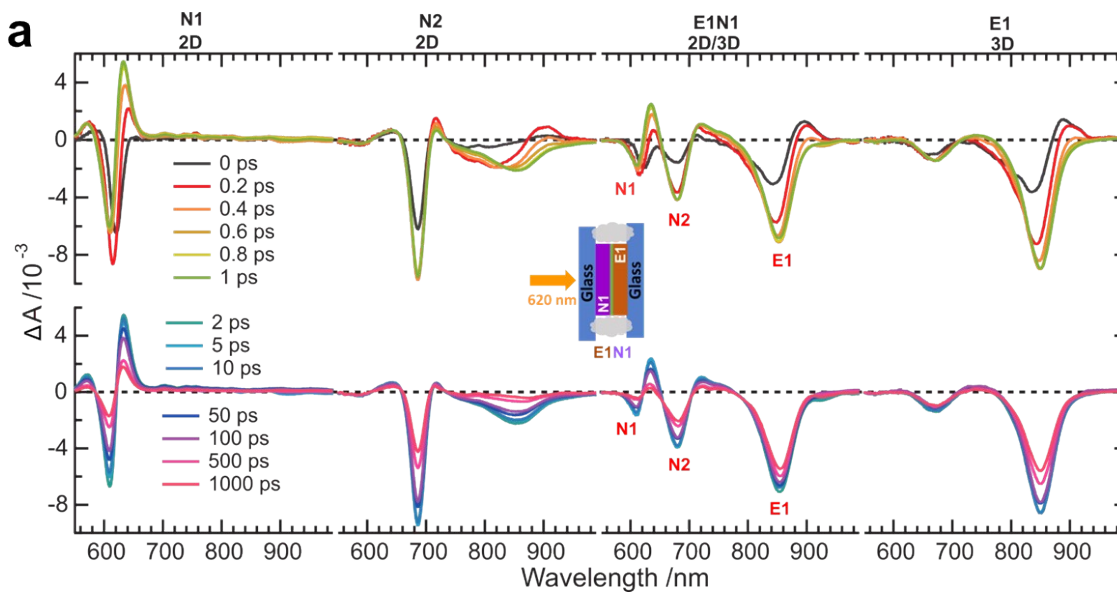


Fig.S6 Normalized Photoluminescence (PL) spectra obtained due to front (E1 side) and back (N1 side) excitation positions of the stacked film from day 1 to day 30. (a) E1N1-BA, (b) E1N1-HA, (c) E1N1-OA, and (d) E1N1-PEA.



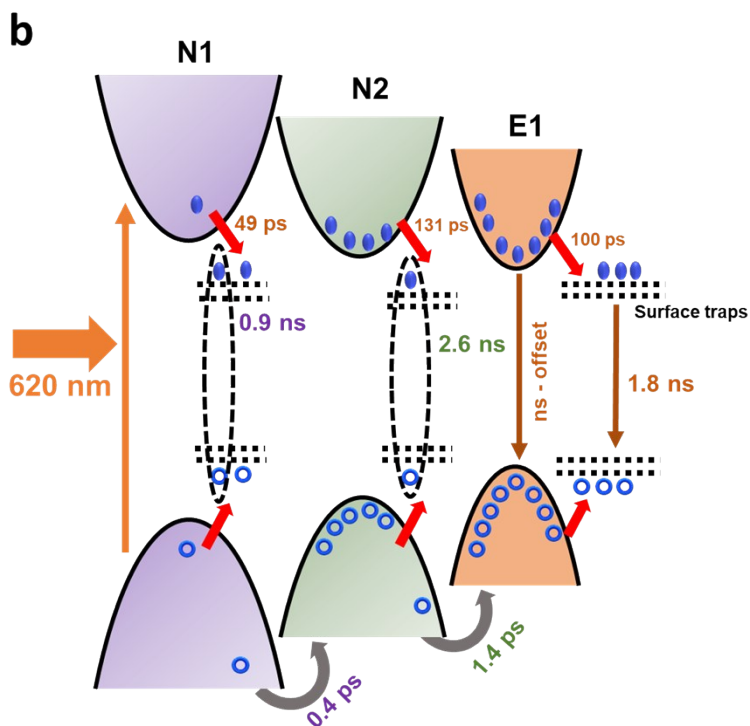


Fig. S7 (a) Femtosecond-transient absorption spectroscopy (fs-TAS) of N1, N2, E1N1-BA (Day 4) and E1 using 620 nm excitation light. (b) carrier relaxation schemes derived fs-TAS experiment carried out at 620 nm excitation light.

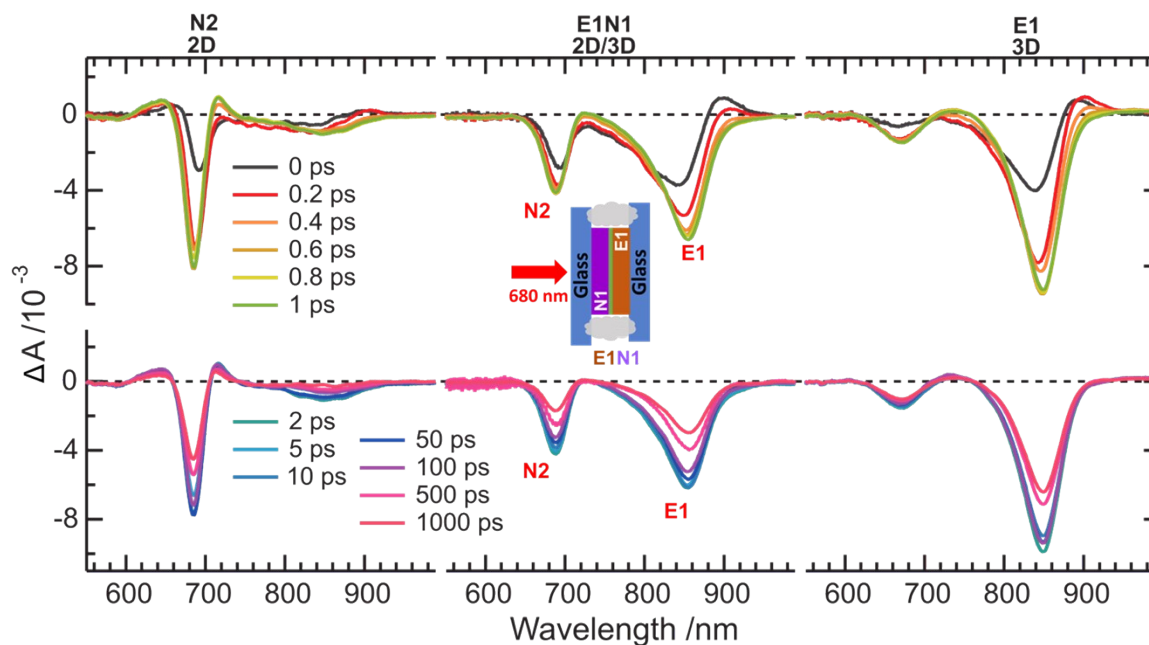


Fig. S8 Femtosecond-transient absorption spectroscopy (fs-TAS) of N2, E1N1-BA (Day 4) and E1 using 680 nm excitation light.

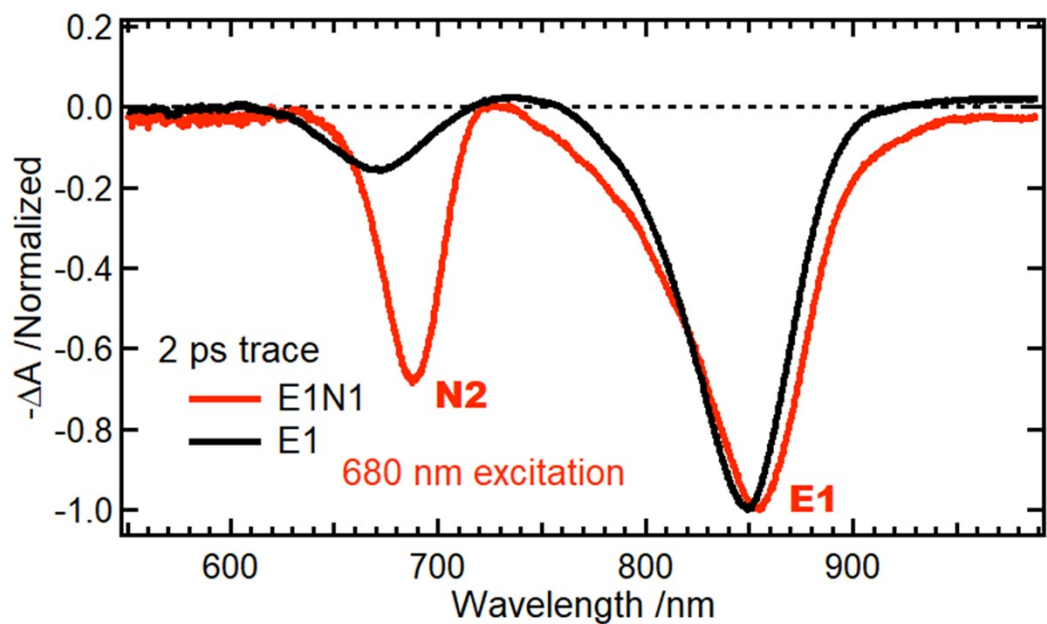


Fig. S9 Comparison of fs-TAS at 2 ps delay position for E1N1-BA (Day 4) and E1.

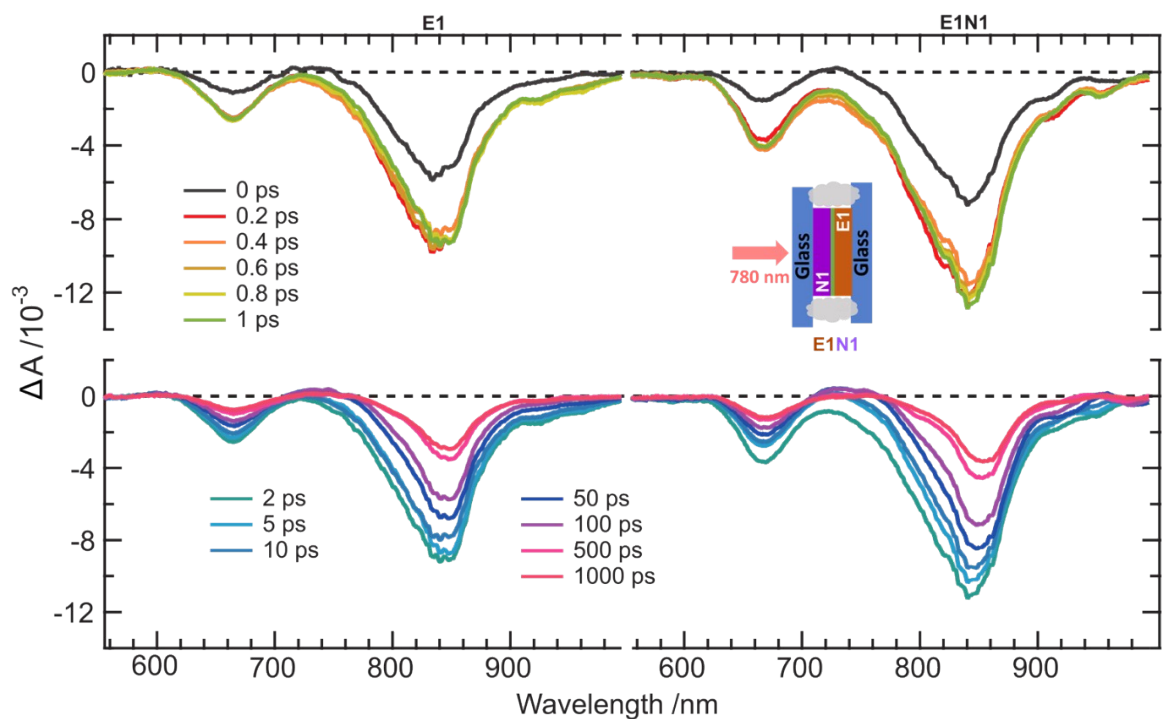


Fig. S10 Femtosecond-transient absorption spectroscopy (fs-TAS) of E1 and E1N1-BA (Day 4) using 780 nm excitation light.

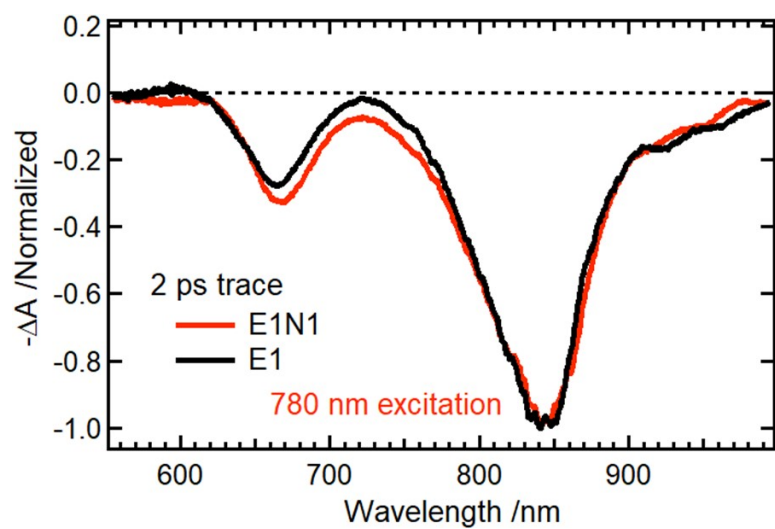


Fig. S11 Comparison of fs-TAS at 2 ps delay position for E1N1-BA (Day 4) and E1.

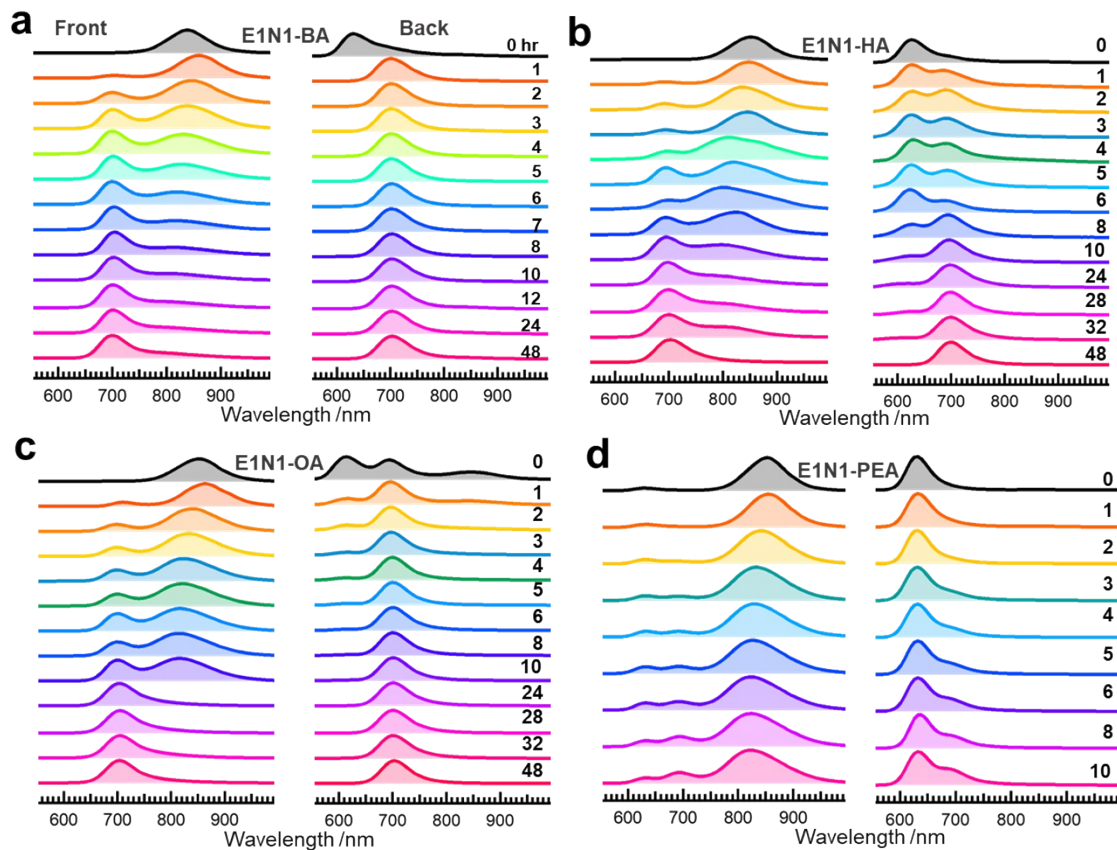


Fig. S12 Normalized Photoluminescence (PL) spectra obtained due to front (E1 side) and back (N1 side) excitation positions of the stacked films under 1 Sun and 50 °C temperature for a period of 48 h for (a) E1N1-BA, (b) E1N1-HA, (c) E1N1-OA, and 10 h for (d) E1N1-PEA.

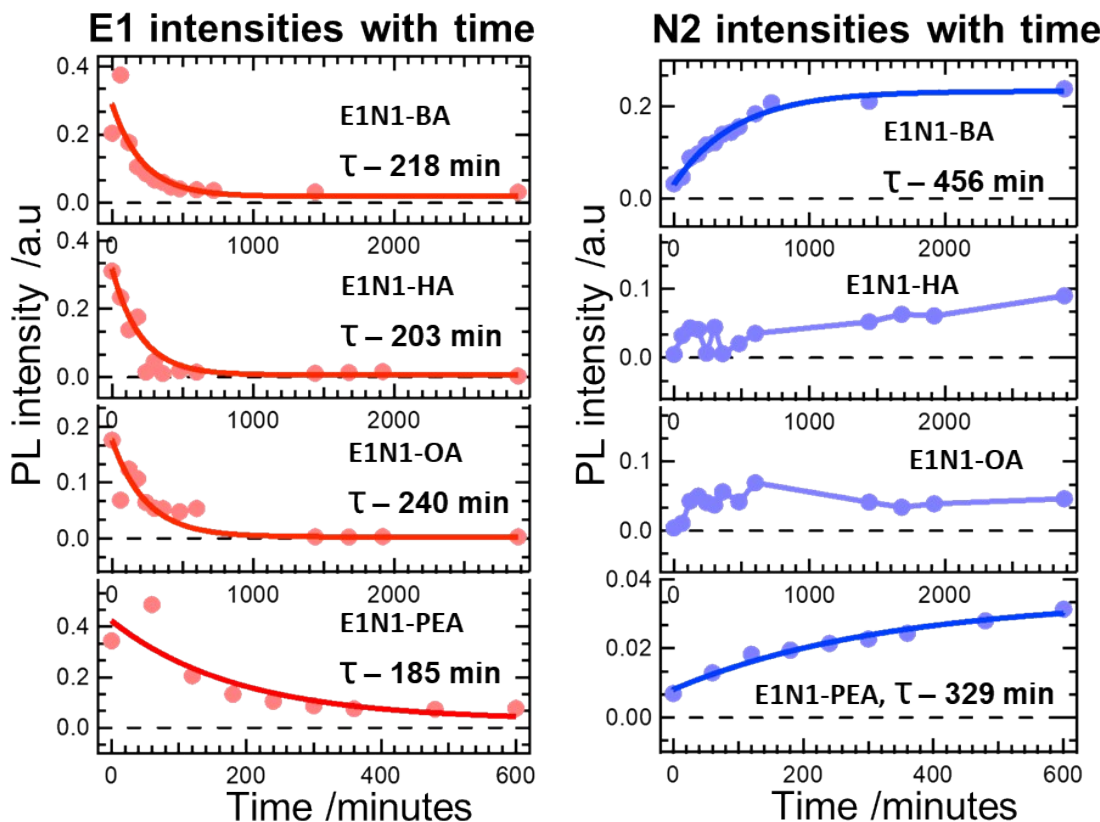


Fig. S13 Time-dependent changes in the PL band intensities of E1 (860 nm) phase and N2 (698 nm) phase for E1N1-BA, E1N1-HA, E1N1-OA, and E1N1-PEA samples as indicated. The PL band intensities were monitored from the PL spectra recorded from the E1 side of the sample.

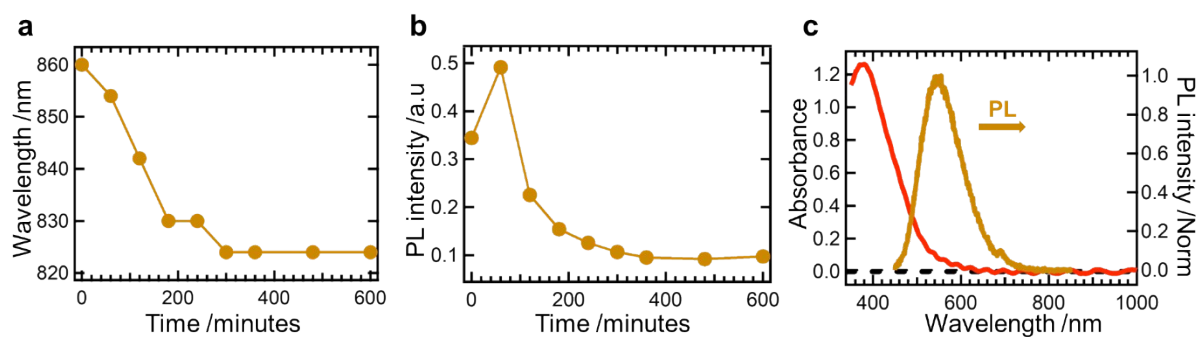


Fig. S14 Time-dependent changes in the PL maxima (a) and band intensities (b) of E1N1-PEA sample measured from the E1 side. (c) UV-vis absorption and PL spectra of E1N1-PEA sample measured at 700 min after the application of light and heat.

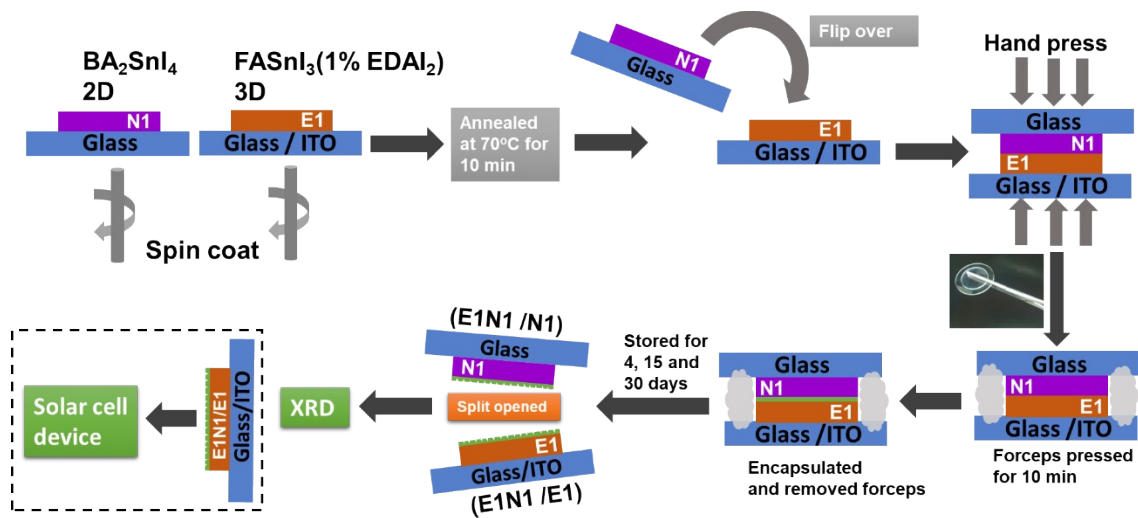


Fig. S15 Schematic demonstration for the stacking sample as shown in Figure 1 of the main text but the stacked sample was split apart into two films ($\text{E1N1}/\text{N1}$ and $\text{E1N1}/\text{E1}$) for XRD characterizations after varied storage periods (4, 15, and 30 days). The $\text{E1N1}/\text{E1}$ film was further used to fabricate Tin perovskite solar cell (TPSC) devices at the storage periods of 4 and 15 days.

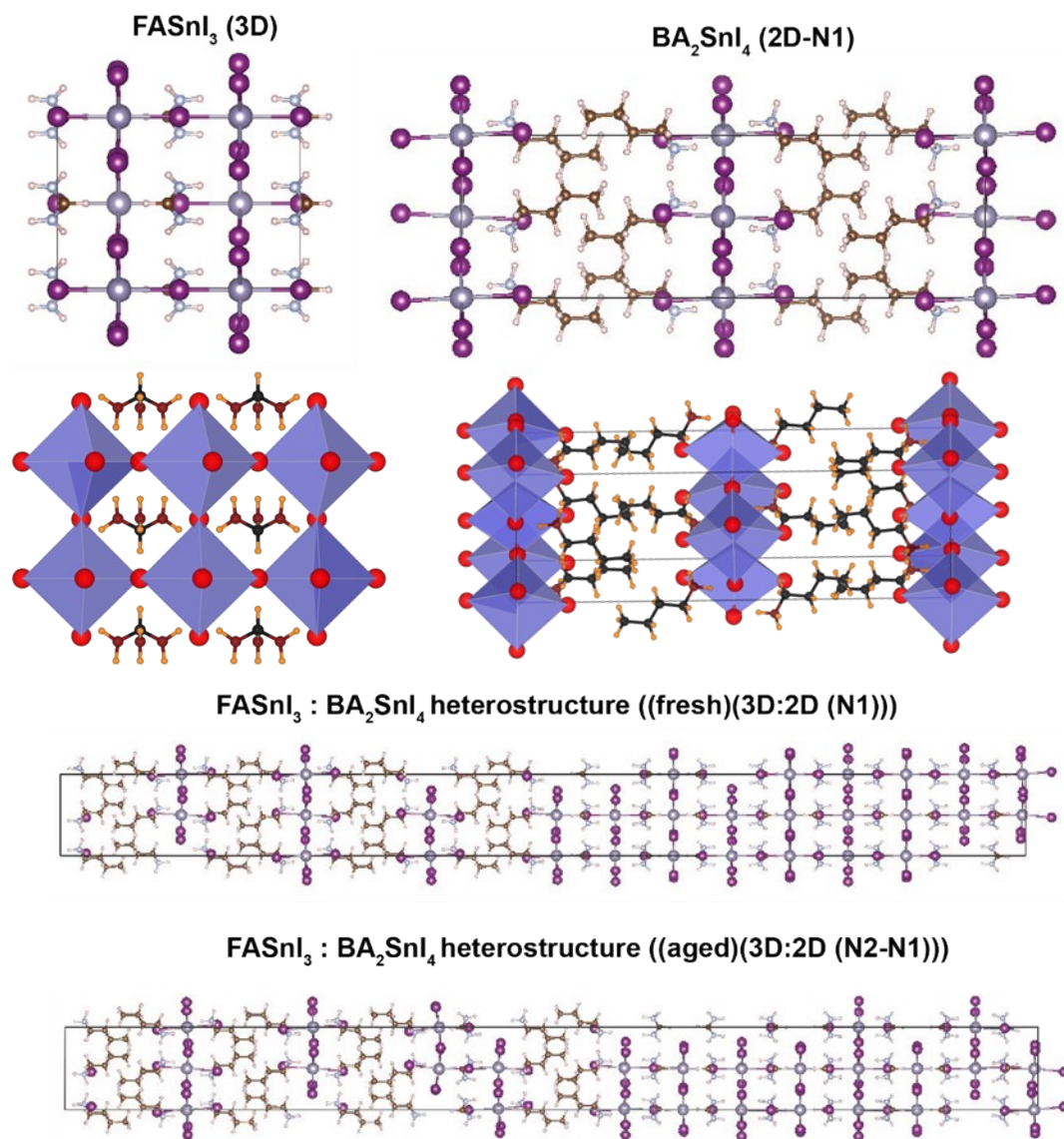


Fig. S16 Optimized structures of FASn₃ (3D), BA₂SnI₄ (N1), 3D-N1 and 3D-N2-N1 heterostructures.

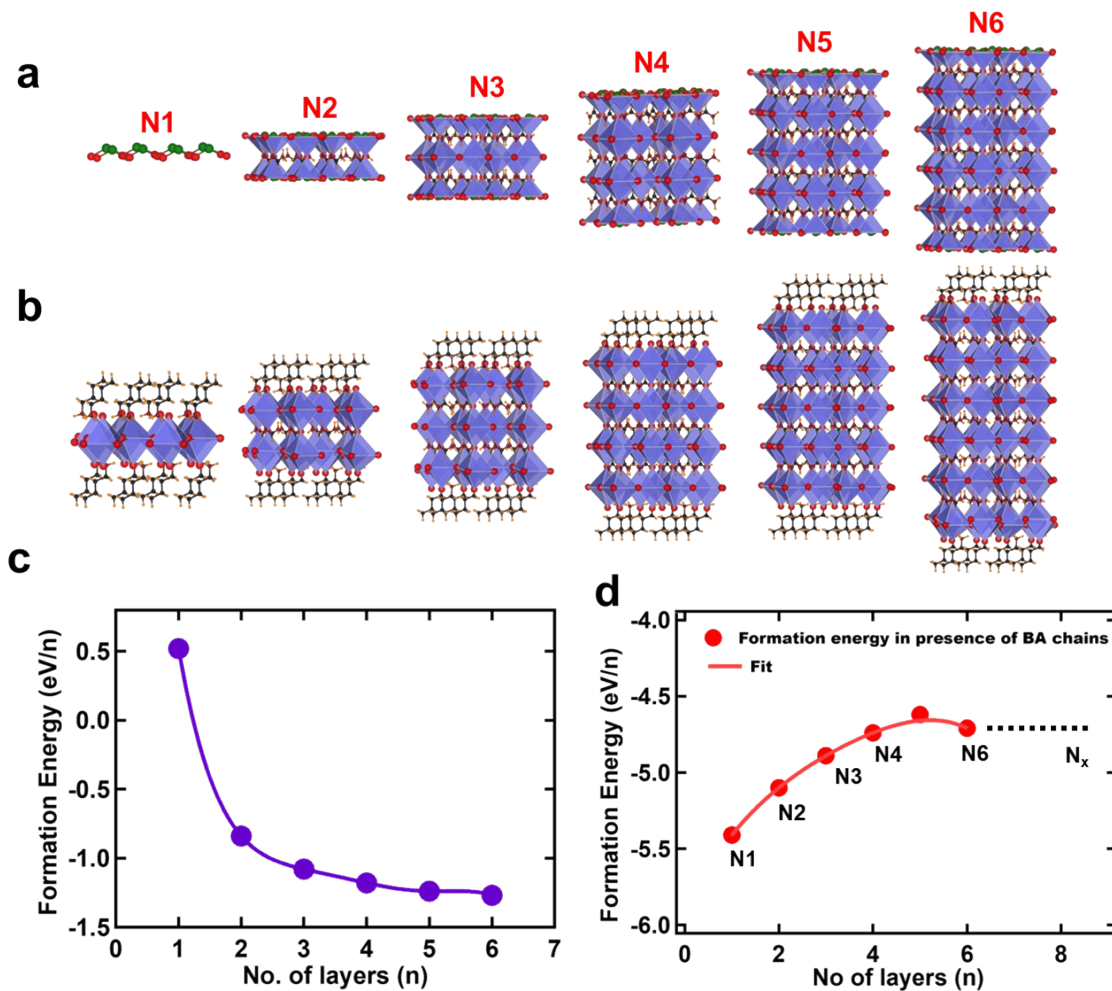


Fig. S17 Optimized structures of two dimensional RP-type Sn perovskites $BA_2FA_{(n-1)}Sn_nI_{(3n+1)}$ ($n = 1$ to 6) (N1-N6) in the forms of (a) slabs of N1-N6 without butylammonium chains and (b) N1-N6 with butylammonium chains (BA). (c) and (d) show formation energies of the corresponding slabs (without BA chains) and layers of N1-N6 structures with BA chains, respectively.

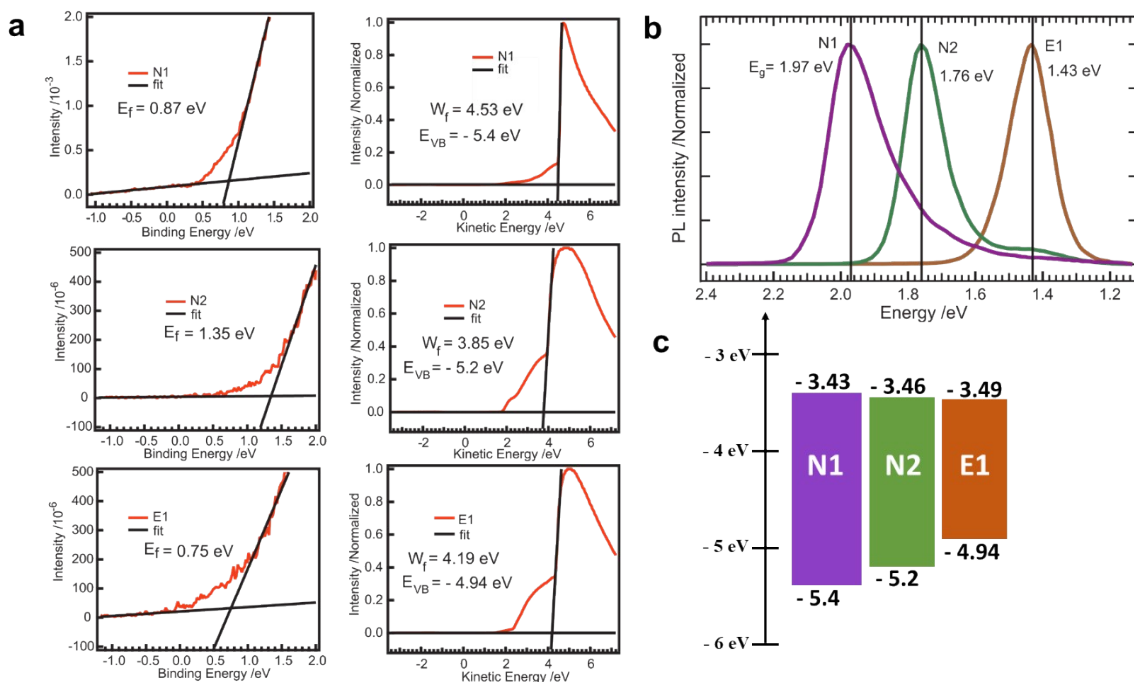


Fig. S18 (a) Ultraviolet photoelectron spectral (UPS) raw data of pristine E1, N1 and N2 samples. The excitation energy was 21.22 eV. (b) shows bandgap estimations for pristine E1, N1(BA) and N2 samples from their corresponding PL^{12, 13} after applying Jacobian correction.¹⁴ The PL curves were fitted with a Gaussian function.

Table S1. Lattice parameters obtained from the optimized structures of FASnI_3 (3D), BA_2SnI_4 (N1), 3D-N1 and 3D-N2-N1 heterostructures (fig. S6).

		a (Å)	b (Å)	c (Å)	α	β	γ
3D	tetragonal	8.73345	8.73345	12.24635	90	90	90
N1	orthorhombic	8.54155	8.39425	27.47657	90	90	90
3D-N1	orthorhombic	8.65752	8.55415	102.33114	90.1	90	90
3D-N2-N1	orthorhombic	8.67717	8.55392	101.87759	90.5	89.9	90

Table S2. Photovoltaic parameters obtained for the TPSC devices fabricated with pristine E1 and the E1N1/E1 films.

Device	J_{sc} (mA cm ⁻²)	Integrated current density (mA cm ⁻²)	V_{oc} (V)	Fill Factor	PCE (%)
Pristine E1	22.7	20.4	0.49	0.69	7.7
E1N1/E1 – 4 days	23.7	21.0	0.50	0.73	8.7
E1N1/E1 – 15 days	24.4	—	0.46	0.55	6.1

Table S3. Comparison of materials and methods used to fabricate 2D/3D tin perovskite heterostructure devices.

Method	Material	J_{sc} (mA cm ⁻²)	V_{oc} (V)	FF	PCE (%)	ref
Layer deposition by Physical stacking	BA ₂ SnI ₄ thin film + FASnI ₃ (1% EDAl ₂) – E1 thin film	23.7	0.49	0.73	8.7	This work
Solution processed (Sequential deposition)	BAI modified GA _{0.2} FA _{0.8} SnI ₃ (1%EDAl ₂) (E1G20)	21.7	0.57	0.73	9.1	15
Solution processed	TEA ₂ FA _{n-1} Sn _n I _{3n+1}	17.05	0.49	0.61	5.17	16
Solution processed	NH ₄ SCN modified PEA _{0.15} FA _{0.85} SnI ₃	22	0.61	0.7	9.41	17
Solution processed	PEA ₂ FA _{n-1} Sn _n I _{3n+1}	24.1	0.52	0.71	9	18
Solution processed (sequential deposition)	PEABr modified FASnI ₃	22.64	0.54	0.64	7.86	19
Vacuum deposition	PEA ₂ FA _{n-1} Sn _n I _{3n+1}	20.32	1	0.67	13.79	20

Solution processed	FPEABr modified FASnI ₃	24.91	0.84	0.71	14.81	21
Solution processed	(PEA) ₂ (FA) _{n-1} Sn _n I _{3n+1}	14.44	0.59	0.69	5.94	11
Solution processed	PEA _{0.08} FA _x SnI ₃	23.1	0.50	0.69	7.99	22
Solution processed (Dip coating)	(TFBA ₂ SnI ₄) _x (FASnI ₃) _{1-x}	21.07	0.70	0.74	10.96	23
Vacuum deposition	PEAI modified FASnI ₃	20.07	0.47	0.74	6.98	24

References

1. E. Jokar, C.-H. Chien, C.-M. Tsai, A. Fathi and E. W.-G. Diau, *Adv. Mater.*, 2019, **31**, 1804835.
2. E. Jokar, C.-H. Chien, A. Fathi, M. Rameez, Y.-H. Chang and E. W.-G. Diau, *Energy Environ. Sci.*, 2018, **11**, 2353-2362.
3. X. Liu, T. Wu, C. Zhang, Y. Zhang, H. Segawa and L. Han, *Adv. Funct. Mater.*, 2021, **31**, 2106560.
4. Z. Wang, F. Wang, B. Zhao, S. Qu, T. Hayat, A. Alsaedi, L. Sui, K. Yuan, J. Zhang, Z. Wei and Z. A. Tan, *J. Phys. Chem. Lett.*, 2020, **11**, 1120-1127.
5. C.-W. Chang, C. K. Chou, I.-J. Chang, Y.-P. Lee and E. W.-G. Diau, *J. Phys. Chem. C*, 2007, **111**, 13288-13296.
6. S. Yamaguchi and H.-O. Hamaguchi, *Appl. Spectrosc.*, 1995, **49**, 1513-1515.
7. G. Kresse and J. Hafner, *Phys. Rev. B*, 1993, **47**, 558-561.
8. S. Grimme, *J. Comput. Chem.*, 2006, **27**, 1787-1799.
9. J. P. Perdew, K. Burke and M. Ernzerhof, *Phys. Rev. Lett.*, 1996, **77**, 3865-3868.
10. T. Shi, H.-S. Zhang, W. Meng, Q. Teng, M. Liu, X. Yang, Y. Yan, H.-L. Yip and Y.-J. Zhao, *J. Mater. Chem. A*, 2017, **5**, 15124-15129.
11. Y. Liao, H. Liu, W. Zhou, D. Yang, Y. Shang, Z. Shi, B. Li, X. Jiang, L. Zhang, L. N. Quan, R. Quintero-Bermudez, B. R. Sutherland, Q. Mi, E. H. Sargent and Z. Ning, *J. Am. Chem. Soc.*, 2017, **139**, 6693-6699.

12. R. L. Milot, G. E. Eperon, H. J. Snaith, M. B. Johnston and L. M. Herz, *Adv. Funct. Mater.*, 2015, **25**, 6218-6227.
13. S. Wang, J. Ma, W. Li, J. Wang, H. Wang, H. Shen, J. Li, J. Wang, H. Luo and D. Li, *J. Phys. Chem. Lett.*, 2019, **10**, 2546-2553.
14. J. Mooney and P. Kambhampati, *J. Phys. Chem. Lett.*, 2013, **4**, 3316-3318.
15. E. Jokar, P.-Y. Cheng, C.-Y. Lin, S. Narra, S. Shahbazi and E. Wei-Guang Diao, *ACS Energy Lett.*, 2021, **6**, 485-492.
16. J.-T. Lin, T.-C. Chu, D.-G. Chen, Z.-X. Huang, H.-C. Chen, C.-S. Li, C.-I. Wu, P.-T. Chou, C.-W. Chiu and H. M. Chen, *ACS Appl. Energy Mater.*, 2021, **4**, 2041-2048.
17. F. Wang, X. Jiang, H. Chen, Y. Shang, H. Liu, J. Wei, W. Zhou, H. He, W. Liu and Z. Ning, *Joule*, 2018, **2**, 2732-2743.
18. S. Shao, J. Liu, G. Portale, H.-H. Fang, G. R. Blake, G. H. Ten Brink, L. J. A. Koster and M. A. Loi, *Adv. Energy Mater.*, 2018, **8**, 1702019.
19. M. Liao, B. B. Yu, Z. Jin, W. Chen, Y. Zhu, X. Zhang, W. Yao, T. Duan, I. Djerdj and Z. He, *ChemSusChem*, 2019, **12**, 5007-5014.
20. T. Wang, H. L. Loi, J. Cao, Z. Qin, Z. Guan, Y. Xu, H. Cheng, M. G. Li, C. S. Lee, X. Lu and F. Yan, *Advanced Science*, 2022, **9**, 2200242.
21. B. B. Yu, Z. Chen, Y. Zhu, Y. Wang, B. Han, G. Chen, X. Zhang, Z. Du and Z. He, *Adv. Mater.*, 2021, **33**, 2102055.
22. S. Shao, M. Nijenhuis, J. Dong, S. Kahmann, G. H. ten Brink, G. Portale and M. A. Loi, *J. Mater. Chem. A*, 2021, **9**, 10095-10103.

23. T. Wu, D. Cui, X. Liu, X. Meng, Y. Wang, T. Noda, H. Segawa, X. Yang, Y. Zhang and L. Han, *Sol. RRL*, 2020, **4**, 2000240.
24. C. Ran, J. Xi, W. Gao, F. Yuan, T. Lei, B. Jiao, X. Hou and Z. Wu, *ACS Energy Lett.*, 2018, **3**, 713-721.